RSC Advances

PAPER

View Article Online
View Journal | View Issue

Cite this: *RSC Adv.*, 2019, **9**, 13808

Critical behavior near room temperature in $La_{0.75}Ca_{0.05}Na_{0.20}MnO_3$ sample

Souhir Bouzidi,[ab] Mohamed Amara Gdaiem, *[a] J. Dhahri [a] and E. K. Hlil[c]

Received 28th January 2019
Accepted 7th April 2019

DOI: 10.1039/c9ra00766k

rsc.li/rsc-advances

The critical behavior of $La_{0.75}Ca_{0.05}Na_{0.20}MnO_3$ was studied at around room temperature *via* magnetization measurements. From the relative slope, we deduced that the Tricritical Mean-Field model was the most suitable model. The estimated critical exponents were found to be $\beta = 0.24 \pm 0.004$, $\gamma = 0.98 \pm 0.065$ and $\delta = 5.08$ at $T_C = 300$ K. These critical exponents satisfied the Widom scaling relation $\delta = 1 + \gamma/\beta$, implying the reliability of our values. Based on the critical exponents, the magnetization–field–temperature ($M-\mu_0H-T$) data around T_C collapsed into two curves, obeying the single scaling equation $M(H,\varepsilon) = \varepsilon^{\beta} f_{\pm}\left(\frac{H}{\varepsilon^{\beta+\gamma}}\right)$ with $\varepsilon = (T - T_C)/T_C$ being the reduced temperature. These results suggest short-range interaction in our sample.

1. Introduction

Over the past few years, the colossal magnetoresistance (CMR) effect in doped manganites has attracted the attention of many researchers owing to their promising physical properties and potential applications around the Curie temperature T_C, such as memory recording, field sensors and magnetic reading heads.[1–3] In general, the perovskite structure shows a distortion from the ideal structure (cubic) to a rhombohedral or orthorhombic structure, which is mainly caused by the Jahn–Teller (JT) effect following the deformation of the MnO_6 octahedron. Particularly, the low-doped $La_{1-x}Sr_xMnO_3$ and $La_{1-x}Ca_xMnO_3$ samples have extraordinary electronic and magnetic properties and are good candidates for technological applications.[4,5] These materials are characterized by an insulator (I)–metal (M) transition and paramagnetic (PM)–ferromagnetic (FM) transition, which leads to the CMR effect. These properties have been explained by the double-exchange (DE) interaction,[6] phase separation[7] and JT effects, which represent the strong electron–phonon interaction.[8] Recently, many studies have investigated the critical behaviors of manganites around the Curie temperature (T_C) to understand their transition nature (first or second order) and the universality class. Historically, the transition from PM-I to the FM-M state has been elucidated by the Zener DE theory.[6] The analysis of the critical behaviors around the T_C is a powerful tool to understand the interaction mechanism responsible for the transition. Therefore, it is important to study in detail the critical exponents in the PM–FM region. Initially, critical phenomena in the DE model were associated with the long-range Mean-Field theory.[9] Subsequently, Motome and Furulawa proposed that the critical behavior could be associated to the short-range Heisenberg universality class.[10] Several experimental studies on critical phenomena are still controversial concerning their Mean-Field values,[11] short-range Heisenberg interaction,[12] 3-D Ising values,[13] and others models which are not classified into any universality class ever known.[14] In general, the critical exponent β varied from 0.3 to 0.5, while the reported values for exponent γ varied from 1 to 1.4. Currently, there are four models that can be defined and used to explain the critical properties in magnetic compounds. These models are the 3D-Heisenberg ($\beta = 0.365$), Mean-Field ($\beta = 0.5$), Tricritical Mean Field ($\beta = 0.25$) and 3D-Ising ($\beta = 0.325$) models. It is noteworthy that the critical phenomenon in the PM–FM region raised important fundamental discussions. Previously,[15] we studied the magnetic and magnetocaloric properties of $La_{0.75}Ca_{0.05}Na_{0.20}MnO_3$ samples. We noticed that our sample displays a FM–PM transition around room temperature. According to the magnetocaloric study, a large magnetic entropy change was observed, with a maximum of 6.01 J kg^{-1} K^{-1}. In addition, it has an important relative cooling ability, which was found to be 225 J kg^{-1}.[15] These results indicate that the material can be a good potential candidate in the refrigeration domain.

In this study, we present the first detailed dc magnetization study of the critical phenomena in a DE FM, $La_{0.75}Ca_{0.05}Na_{0.20}MnO_3$. We determined the T_C and the critical exponents γ, β and δ and tested them for scaling.

[a]*Laboratoire de la Matière Condensée et des Nanosciences, Département de Physique, Faculté des Sciences de Monastir, Université de Monastir, Avenue de l'Environnement, Monastir 5019, Tunisia. E-mail: gdaiem_mohamed@hotmail.fr; Fax: +21673500280; Tel: +21629523640*

[b]*Higher School of Science and Technology of Hammam Sousse, University of Sousse, Tunisia*

[c]*Institut Néel, CNRS et Université Joseph Fourier, BP 166, F-38042, Grenoble Cedex 9, France*

2. Experimental details

The $La_{0.75}Ca_{0.05}Na_{0.20}MnO_3$ polycrystalline sample was prepared by the flux method, using NaCl as a flux.[15] The crystal structure of the studied powder was checked by X-ray diffraction, which confirmed that the sample crystallized in the rhombohedral structure with the $R\bar{3}c$ space group and had a detectable secondary phase of Mn_3O_4.[15] The relative amount of Mn_3O_4 as determined from the XRD patterns of the sample was found to be 10%. To extract the critical exponent of the samples accurately, the magnetic isotherm for the sample was measured in the range of 0–5 T, in the vicinity of the PM to FM phase transition. The isothermals were corrected by a demagnetization factor D that was determined by a standard procedure from the low-field dc magnetization measurement at low temperatures ($H = H_{app} - DM$).

3. Results and discussion

In our earlier work,[15] we showed that for $La_{0.75}Ca_{0.05}Na_{0.20}MnO_3$, the field-cooled (FC) magnetization *versus* temperature under an applied magnetic field of 0.05 T demonstrated a magnetic transition from the PM to FM state at its T_C, with the decrease in temperature; the T_C value was found to be 300 K. To introduce the FM state in manganite oxide type perovskite, the existence of the Mn^{3+}–Mn^{4+} mixed valence is necessary. Ferromagnetism is caused by the exchange energy; this favors electrons with parallel spins. A deeper insight into the magnetic phase transition may be obtained by analyzing the critical phenomena. Based on Banerjee's criterion, a positive slope reflects a second order magnetic transition, while a negative one reflects a first order magnetic transition. From Fig. 1, we obtained a positive slope for our sample. This indicates that $La_{0.75}Ca_{0.05}Na_{0.20}MnO_3$ undergoes a second order PM–FM transition. It is well known that a magnetic system showing a second order PM–FM transition, around T_C, can be described by a set of interrelated critical exponents.

According to the scaling hypothesis, for a second-order phase transition around T_C, the critical exponents β (associated with the spontaneous magnetization $M_S(T) = \lim_{H\to 0} M$ just below T_C), γ (relevant to the initial magnetic susceptibility χ_0, $\chi_0^{-1}(T) = \lim_{H\to 0}(\mu_0 H/M)$ just above T_C), and δ (associated with the critical isotherm $M(T_C, \mu_0 H)$ at T_C) are given as:[16]

$$M_S(T) = M_0(-\varepsilon)^{\beta},\ \varepsilon < 0,\ T < T_C \quad (1)$$

$$\chi_0^{-1}(T) = \left(\frac{h_0}{M_0}\right)\varepsilon^{\gamma},\ \ \varepsilon > 0,\ T > T_C \quad (2)$$

$$M = D(\mu_0 H)^{\frac{1}{\delta}},\ \ \varepsilon = 0,\ T = T_C \quad (3)$$

where β is associated with the spontaneous magnetization M_S, γ is associated with the initial magnetic susceptibility χ_0, δ is associated with the critical magnetization isotherm at T_C, $\varepsilon = (T - T_C)/T_C$ is the reduced temperature, $\mu_0 H$ is the demagnetization adjusted magnetic field and M_0, h_0/M_0, and D the critical amplitudes. According to the critical region theory, the reduced magnetic equation of state can be expressed as

$$M(\mu_0 H, \varepsilon) = \varepsilon^{\beta} f_{\pm}\left(\frac{\mu_0 H}{\varepsilon^{\beta+\gamma}}\right) \quad (4)$$

where $f_{\pm}$ are the regular analytical functions with f_+ for $T > T_C$, and f_- for $T < T_C$.[17,18]

Eqn (4) implies that $M/|\varepsilon|^{-\beta}$ as a function $\mu_0 H/|\varepsilon|^{-(\beta+\gamma)}$, falls on two universal curves, one for $T > T_C$, and the other for $T < T_C$. In general, four models can be defined according to the values of the critical exponents; 3D-Heisenberg model ($\beta = 0.365$ and $\gamma = 1.336$), Mean-Field model ($\beta = 0.5$ and $\gamma = 1$), Tricritical Mean-Field model ($\beta = 0.25$ and $\gamma = 1$) and the 3D-Ising model ($\beta = 0.325$ and $\gamma = 1.24$). The different models are collected in Table 1.

The Modified Arrott Plot (MAP) is a conventional method to estimate the critical exponents and critical temperature.[20] According to this method, isotherms plotted in the form of M^2 as function of $\mu_0 H/M$ constitute a set of parallel straight lines around T_C. The line at $T = T_C$ should pass through the origin. It is worth mentioning that the Arrott plot assumes the critical exponents following the Mean-Field theory. In the present case, the curves in the Arrott plot are non-linear and concave as shown in Fig. 1. For this reason, we tried to analyze our data according to the MAP method, based on the Arrott–Noakes equation. This method is based on the equation of state:[21]

$$(\mu_0 H/M)^{1/\gamma} = a\frac{(T - T_C)}{T} + b(M)^{\frac{1}{\beta}} \quad (5)$$

where a and b are constants.

Fig. 2 displays MAP at different temperatures for our sample using three models of critical exponents: Fig. 2(a) 3D-Heisenberg model, Fig. 2(b) Tricritical Mean-Field model, and Fig. 2(c) 3D-Ising model. One can see that all models yield quasi straight lines. Here, it is difficult to define which model is the most appropriate for determining the critical exponents. To distinguish which model better describes this system, we calculated the relative slope (RS) defined at the critical point: RS $= S(T)/S(T_C)$. The $S(T)$ and $S(T_C)$ are the slope for a given T close to T_C and the slope at $T = T_C$, respectively. The most appropriate model should be close to 1 (unity).[22] The RS as function of the temperature curve for all models is shown in Fig. 3. From this

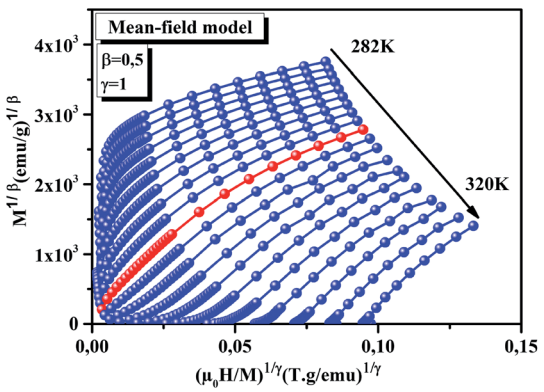

Fig. 1 A set of typical M^2 *vs.* $\mu_0 H/M$ plots, for the $La_{0.75}Ca_{0.05}Na_{0.20}MnO_3$ sample.

Table 1 Comparison of critical exponents of the $La_{0.75}Ca_{0.05}Na_{0.20}MnO_3$ sample with various theoretical models and earlier results on manganites

Samples	Technique	T_C (K)	β	γ	δ	Ref.
$La_{0.75}Ca_{0.05}Na_{0.20}MnO_3$	MAP	299.48 ± 0.12K	0.24 ± 0.004	0.98 ± 0.065	5.08	This work
	KF	299.04 ± 0.03	0.22 ± 0.006	1.034 ± 0.063	5.70	This work
	CI (exp)	300	—	—	4.86 ± 0.004	This work
Mean Field model	Theory	—	0.5	1	3	18
3D-Heisenberg model	Theory	—	0.365	1.336	4.8	18
3D Ising model	Theory	—	0.325	1.24	4.82	18
Tricritical Mean Field model	Theory	—	0.25	1	5	19
$La_{0.1}Nd_{0.6}Sr_{0.3}MnO_3$		249.36 ± 0.04	0.248 ± 0.006	1.066 ± 0.002	5.298	25
$Nd_{0.7}Sr_{0.3}MnO_3$		238	0.271 ± 0.006	0.922 ± 0.016	4.5	26
$La_{0.7}Ba_{0.3}MnO_3$		311.2	0.54 ± 0.02	1.04 ± 0.04	3.08 ± 0.04	27
$La_{0.7}Ca_{0.3}Mn_{0.91}Ni_{0.09}O_3$		199.5 ± 0.1	0.171 ± 0.006	0.976 ± 0.012	6.7	28
$La_{0.67}Pb_{0.33}Mn_{0.97}Co_{0.03}O_3$		345	0.233 ± 0.002	1.06 ± 0.06	5.52 ± 0.04	29
$La_{0.6}Ca_{0.4}MnO_3$		265.5	0.25	1.03	5	30
$La_{0.7}Sr_{0.3}MnO_3$		354	0.37 ± 0.04	1.22 ± 0.03	4.25 ± 0.2	2

figure, it can be seen that the Tricritical Mean-Field model is the best to describe our system.

The high field straight line portions of the isotherms in Fig. 2(b) can be linearly extrapolated to obtain the spontaneous magnetization $M_S(T, 0)$ and the inverse susceptibility $(\chi_0^{-1}(T))$. The temperature dependence of $M_S(T, 0)$ and $\chi_0^{-1}(T)$ for our sample are shown in Fig. 4. The continuous curves in Fig. 4 denote the power law fitting of $M_S(T, 0)$ and $\chi_0^{-1}(T)$ as a function of temperature according to eqn (1) and (2), respectively. This gives the values of $\beta = 0.24 \pm 0.004$ with $T_C = 299.48 \pm 0.12$ K and $\gamma = 0.98 \pm 0.065$, with $T_C = 299 \pm 0.66$ K. Moreover, β, γ and T_C can be also determined from the Kouvel–Fisher (KF) method[23] based on the following expressions:

$$\left[\frac{M_S}{dM_S/dT}\right] = \frac{[T - T_C]}{\beta} \quad (6)$$

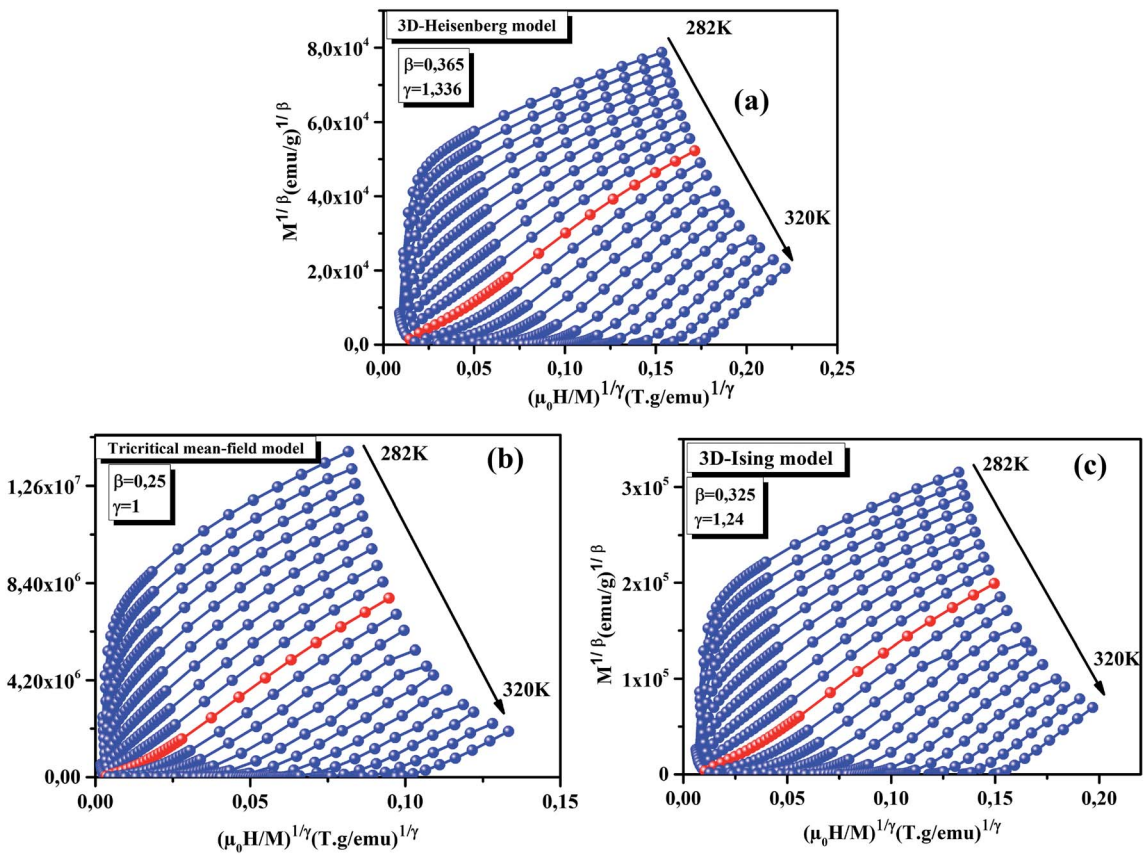

Fig. 2 Modified Arrott plots: ($M^{1/\beta}$ *vs.* $\mu_0 H/M$) for the $La_{0.75}Ca_{0.05}Na_{0.20}MnO_3$ sample.

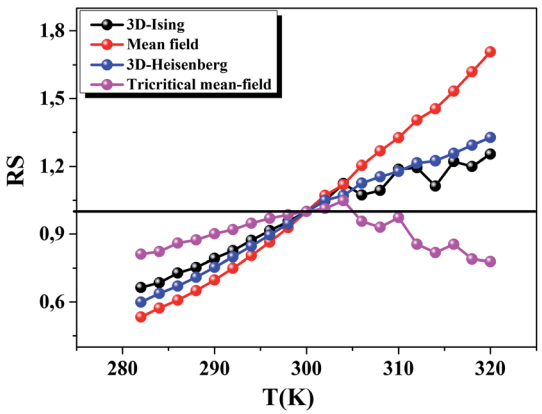

Fig. 3 RS *versus* temperature for the $La_{0.75}Ca_{0.05}Na_{0.20}MnO_3$ sample.

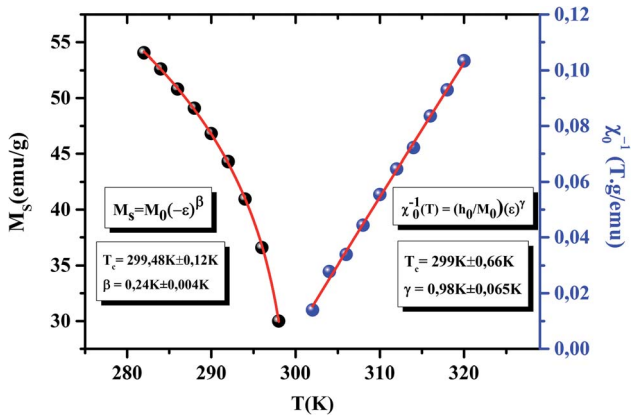

Fig. 4 M_S (left) and χ_0^{-1} (right) as function of temperature for the $La_{0.75}Ca_{0.05}Na_{0.20}MnO_3$ sample (solid lines are fits to the model).

$$\left[\frac{\chi_0^{-1}}{\mathrm{d}\chi_0^{-1}/\mathrm{d}T}\right] = \frac{[T - T_C]}{\gamma} \tag{7}$$

According to eqn (6) and (7), we plotted $M_S(T)[\mathrm{d}M_S(T)/\mathrm{d}T]^{-1}$ and $\chi_0^{-1}(T)[\mathrm{d}\chi_0^{-1}(T)/\mathrm{d}T]^{-1}$ from the obtained $M_S(T)$ and $\chi_0^{-1}(T)$ curves, which should yield straight lines with slopes $1/\beta$ and $1/\gamma$ respectively. The T_C values are obtained from the intercepts on the T axis. The KF curve for our sample is shown in Fig. 5. Besides, the parameters obtained from the linear fitting are found to be $\beta = 0.220 \pm 0.006$ with $T_C = 299.04 \pm 0.03$ K and $\gamma = 1.034 \pm 0.063$ with $T_C = 298.53 \pm 0.06$ K for our sample. Obviously, the values of the critical exponents and T_C obtained using the KF method are in agreement with those obtained using the MAP of the Tricritical model. The value of δ can be determined from the linear fitting of the critical isotherm $M(T_C, \mu_0H)$. Fig. 6 displays $M(\mu_0H)$ curve at 300 K, chosen as the critical isotherm based on the previous discussion. The inset (a) of Fig. 6 shows the same curve M *vs.* μ_0H on the ln–ln scale. The solid straight line with a slope $1/\delta$ is the fitting result using eqn (3). From the linear fit, we obtained the third critical exponent δ, which is found to be 4.86 ± 0.004. According to the statistical theory, these three critical exponents must fulfill the Widom scaling relation:[24]

$$\delta = 1 + \gamma/\beta \tag{8}$$

Using this scaling relation and the estimated values of β and γ, we found that δ value is close to the value directly determined from the critical isotherm at T_C, implying that the obtained β and γ values are consistent. All the obtained critical exponents determined from the various methods are listed in Table 1 and compared with other works.[2,25–30]

Furthermore, the relationship between critical exponents can also be verified by plotting $M(T_C)$ as a function of $\mu_0H^{1/\delta}$ (inset (b) of Fig. 6). The plot shows a linear curve, which proves that the different critical exponents and T_C obey the Widom scaling relation, and that the determined β and γ values are reliable. In order to make sure of the reliability of the determined critical exponent values and check our data in the critical region, we plotted $M|\varepsilon|^{\beta}$ as a function of $\mu_0H|\varepsilon|^{(\beta+\gamma)}$ in the low and high field region. The plots are shown in Fig. 7, using the critical exponents obtained *via* the KF method. From this figure,

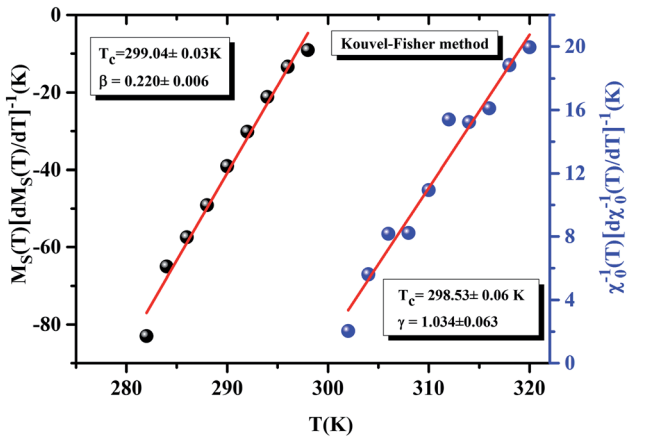

Fig. 5 K–F plots for the $La_{0.75}Ca_{0.05}Na_{0.20}MnO_3$ sample (solid lines are fits to the model).

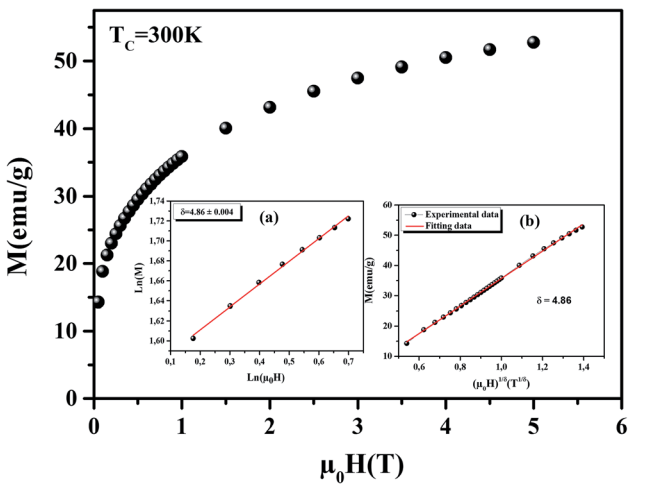

Fig. 6 M *vs.* μ_0H plot for the $La_{0.75}Ca_{0.05}Na_{0.20}MnO_3$ sample at T_C = 300 K. The inset (a) displays the same plot in ln–ln scale and the inset (b) shows $M(T_C)$ as function of $\mu_0H^{1/\delta}$.

we observe that all the points fall into two curves, one below T_C and another one above T_C. This suggests that the values of the exponents and that of the T_C are reasonably accurate. The inset of Fig. 7 displays the same plot on a log–log scale. One can see the same behavior is observed in Fig. 7. This confirms that our obtained critical exponents and T_C are in agreement with the scaling hypothesis.[16] Besides, the reliability of the critical exponents can be tested by other rigorous methods. The first method is based on the m^2 *vs.* $\mu_0 h/m$ curve.[18] Here, $m = M(\mu_0 H, \varepsilon)\varepsilon^{-\beta}$ and $h = \mu_0 H \varepsilon^{-(\beta+\gamma)}$ are the renormalized magnetization and field, respectively. The m^2 *vs.* $\mu_0 h/m$ curve for our sample is shown in Fig. 8. We can see from this figure that all the data still fall on two separate curves. These results confirm that the critical exponents can generate the scaling equation of state for $La_{0.75}Ca_{0.05}Na_{0.20}MnO_3$.

The second method is shown in Fig. 9. According to the scaling equation of state:[31]

$$\left(\frac{\mu_0 H}{M^{\delta}} = h\frac{\varepsilon}{M^{\frac{1}{\beta}}}\right) \quad (9)$$

where h is the scaling function. Based on this, we can confirm the reliability of the used T_C and the critical exponents. The hypothesis from the scaling eqn (9) is that all the experimental data points should collapse onto a universal curve.[32] Fig. 9 displays $M/(\mu_0 H)^{1/\delta}$ *vs.* $\varepsilon/(\mu_0 H)^{1/\beta+\gamma}$, using the critical exponents and the T_C determined from the KF method and the critical isotherm. It is clear that our curves collapse onto a universal curve, which confirms that the critical exponents are appropriate.

Moreover, the reliability of the critical exponents can be checked by an equation proposed by Franco *et al.*[33] In fact, for magnetic systems, the scaling equation of state takes the form:

$$-\Delta S_M(\mu_0 H, T) = (\mu_0 H)^{(1-\alpha)/\Delta} g\left(\frac{\varepsilon}{(\mu_0 H)^{1/\Delta}}\right) \quad (10)$$

Eqn (10) is based on the relationship between the critical exponents and the magnetic entropy change, where $\Delta = \beta + \gamma$ and $\alpha + 2\beta + \gamma = 2$ are the usual critical exponents. According to eqn (10) and using the critical exponents from MAP, Fig. 10 shows $\frac{-\Delta S_M(\mu_0 H, T)}{(\mu_0 H)^{(1-\alpha)/\Delta}}$ *vs.* $\frac{\varepsilon}{(\mu_0 H)^{1/\Delta}}$ plot. We can see that all $(-\Delta S_M)$ curves collapse on a single curve. This indicates

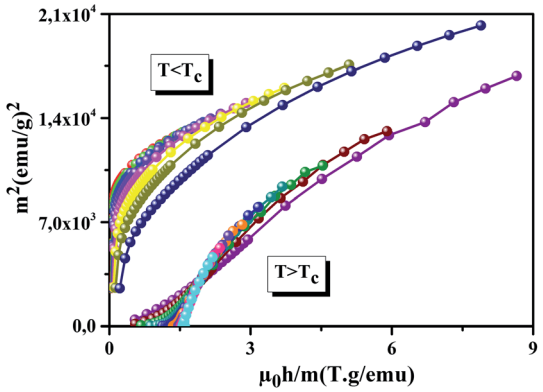

Fig. 8 The renormalized magnetization m^2 *versus* $\mu_0 h/m$ for the $La_{0.75}Ca_{0.05}Na_{0.20}MnO_3$ sample.

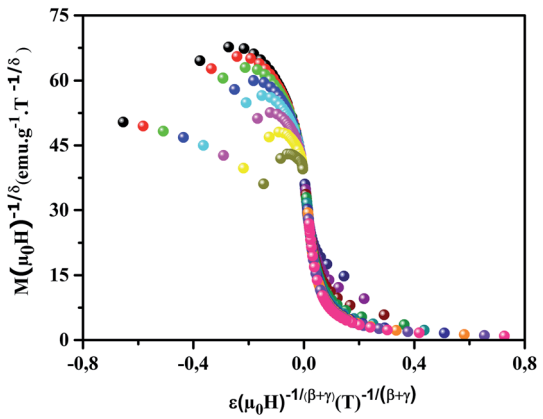

Fig. 9 $M(\mu_0 H)^{-1/\delta}$ as function of $\varepsilon(\mu_0 H)^{-1/(\beta+\gamma)}$ for the $La_{0.75}Ca_{0.05}Na_{0.20}MnO_3$ sample in the critical region, at different temperatures.

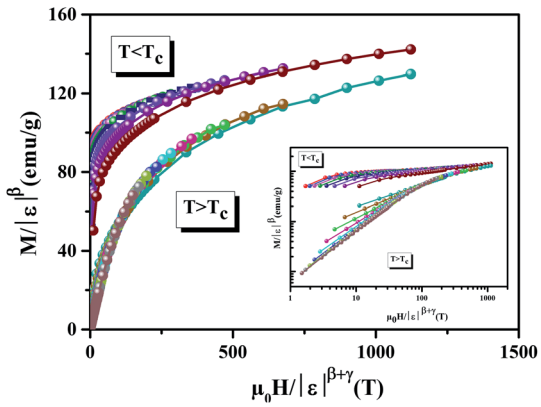

Fig. 7 Scaling plot below and above T_C for the $La_{0.75}Ca_{0.05}Na_{0.20}MnO_3$ sample. The inset shows the same plots on a ln–ln scale.

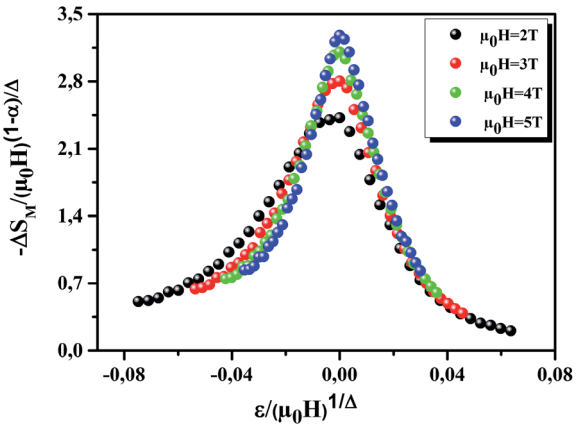

Fig. 10 The variation of $\frac{-\Delta S(\mu_0 H, T)}{(\mu_0 H)^{(1-\alpha)/\Delta}}$ *vs.* $\frac{\varepsilon}{(\mu_0 H)^{1/\Delta}}$.

excellent agreement between the critical exponents and the scaling hypothesis near the magnetic transition.

4. Conclusion

In the present study, we have comprehensively studied the critical phenomenon at the FM–PM phase transition in a polycrystalline manganite of $La_{0.75}Ca_{0.05}Na_{0.20}MnO_3$ *via* dc magnetization. The values of the critical exponents for our sample were extracted using the MAP method, KF method and critical isotherm analysis. Interestingly, the obtained exponent values are very close to the values expected for the universality class of the Tricritical Mean Field model. The validity of the obtained critical exponents using the various methods was confirmed by the Widom scaling relation and the universal scaling hypothesis.

Conflicts of interest

The authors declare no conflict of interest.

References

1 K. Chahara, T. Ohno, M. Kasai and Y. Kosono, *Appl. Phys. Lett.*, 1993, **63**, 1990–1992.
2 K. Ghosh, C. J. Lobb, R. L. Greene, S. G. Karabashev, D. A. Shulyatev, A. A. Arsenov and Y. Mukovskii, *Phys. Rev. Lett.*, 1998, **81**, 4740–4743.
3 M. S. Kim, J. B. Yang, Q. Cai, X. D. Zhou, W. J. James, W. B. Yelon, P. E. Parris, D. Buddhikot and S. K. Malik, *Phys. Rev. B: Condens. Matter Mater. Phys.*, 2005, **71**, 014433.
4 A. Urushibara, Y. Morimoto, T. Arima, A. Masamitsu, G. Kido and Y. Tokura, *Phys. Rev. B: Condens. Matter Mater. Phys.*, 1995, **51**, 14103–14109.
5 M. McCormack, S. Jin, T. H. Teifel, R. M. Fleming, J. M. Phillips and R. Ramesh, *Appl. Phys. Lett.*, 1994, **64**, 3045–3047.
6 C. Zener, *Phys. Rev.*, 1951, **82**, 403–405.
7 M. Uehara, S. Mori, C. H. Chen and S. W. Cheong, *Nature*, 1999, **399**, 560–563.
8 X. G. Li, R. K. Zheng, G. Li, H. D. Zhou, R. X. Huang, J. Q. Xie and Z. D. Wang, *Europhys. Lett.*, 2002, **60**, 670–676.
9 K. Kubo and N. Ohata, *J. Phys. Soc. Jpn.*, 1972, **33**, 21–32.
10 Y. Motome and N. Furulawa, *J. Phys. Soc. Jpn.*, 2001, **70**, 1487–1490.
11 S. Taran, B. K. Chaudhuri, S. Chatterjee, H. D. Yang, S. Veeleshwar and Y. Y. Chen, *J. Appl. Phys.*, 2005, **98**, 103903.
12 A. Tozri, E. Dhahri and E. K. Hlil, *Phys. Lett. A*, 2011, **375**, 1528–1533.
13 L. Chen, J. H. He, Y. Mei, Y. Z. Cao, W. WXia, H. F. Xu, Z. W. Zhu and Z. A. Xu, *Phys. B*, 2009, **404**, 1879–1882.
14 D. Kim, B. L. Zink, F. Hellman and J. D. Coey, *Phys. Rev. B: Condens. Matter Mater. Phys.*, 2002, **65**, 214424–214431.
15 S. Bouzidi, M. A. Gdaiem, J. Dhahri and E. K. Hlil, *RSC Adv.*, 2019, **9**, 65–76.
16 H. E. Stanley, *Introduction to Phase Transitions and critical Phenomena*, Oxford University, London, 1971.
17 H. E. Stanley, *Rev. Mod. Phys.*, 1999, **71**, 358–366.
18 S. N. Kaul, *J. Magn. Magn. Mater.*, 1985, **53**, 5–53.
19 K. Huang, *Statistical Mechanics*, Wiley, New York, 2nd edn, 1987.
20 A. Arrott, *Phys. Rev.*, 1957, **108**, 1394–1396.
21 A. Arrott and J. E. Noakes, *Phys. Rev. Lett.*, 1967, **19**, 786–789.
22 A. Schwartz, M. Scheffler and S. M. Anlage, *Phys. Rev. B: Condens. Matter Mater. Phys.*, 2000, **61**, R870–R873.
23 J. S. Kouvel and M. E. Fisher, *Phys. Rev.*, 1964, **136**, 1626–1632.
24 B. Widom, *J. Chem. Phys.*, 1965, **43**, 3898–3905.
25 J. Fan, L. Ling, B. Hong, L. Zhang, L. Pi and Y. Zhang, *Phys. Rev. B: Condens. Matter Mater. Phys.*, 2010, **81**, 144426.
26 T. L. Phan, T. A. Ho, P. D. Thang, Q. T. Tran, T. D. Thanh, N. X. Phuc, M. H. Phan, B. T. Huy and S. C. Yu, *J. Alloys Compd.*, 2014, **615**, 937–945.
27 M. Ziese, *J. Phys.: Condens. Matter*, 2001, **13**, 2919–2934.
28 T. L. Phan, Q. T. Tran, P. Q. Thanh, P. D. H. Yen, T. D. Thanh and S. C. Yu, *Solid State Commun.*, 2014, **184**, 40–46.
29 N. Dhahri, J. Dhahri, E. K. Hlil and E. Dhahri, *J. Magn. Magn. Mater.*, 2012, **324**, 806–811.
30 D. Kim, B. Revaz, B. L. Zink, F. Hellman, J. J. Rhyne and J. F. Mitchell, *Phys. Rev. Lett.*, 2002, **89**, 227202.
31 V. Franco, R. Caballero-Flores, A. Conde, K. E. Knipling and M. A. Willard, *Appl. Phys. Lett.*, 2011, **98**, 102505.
32 R. M'nassri, N. Chniba-Boudjada and A. Cheikhrouhou, *J. Alloys Compd.*, 2015, **640**, 183–192.
33 V. Franco and A. Conde, *Int. J. Refrig.*, 2010, **33**, 465–473.